



## Aspect ratio effects on neoclassical tearing modes from comparison between DIII-D and National Spherical Torus Experiment

R. J. La Haye, R. J. Buttery, S. P. Gerhardt, S. A. Sabbagh, and D. P. Brennan

Citation: [Phys. Plasmas](#) **19**, 062506 (2012); doi: 10.1063/1.4729658

View online: <http://dx.doi.org/10.1063/1.4729658>

View Table of Contents: <http://pop.aip.org/resource/1/PHPAEN/v19/i6>

Published by the [American Institute of Physics](#).

---

### Related Articles

Temporal and spectral evolution of runaway electron bursts in TEXTOR disruptions

[Phys. Plasmas](#) **19**, 092513 (2012)

Modification of  $\Delta'$  by magnetic feedback and kinetic effects

[Phys. Plasmas](#) **19**, 092510 (2012)

Magneto-modulational instability in Kappa distributed plasmas with self-generated magnetic fields

[Phys. Plasmas](#) **19**, 092114 (2012)

Multi-dimensional instability of dust-acoustic solitary waves in a magnetized plasma with opposite polarity dust

[Phys. Plasmas](#) **19**, 093707 (2012)

Nonlinear electron-magnetohydrodynamic simulations of three dimensional current shear instability

[Phys. Plasmas](#) **19**, 092305 (2012)

---

### Additional information on Phys. Plasmas

Journal Homepage: <http://pop.aip.org/>

Journal Information: [http://pop.aip.org/about/about\\_the\\_journal](http://pop.aip.org/about/about_the_journal)

Top downloads: [http://pop.aip.org/features/most\\_downloaded](http://pop.aip.org/features/most_downloaded)

Information for Authors: <http://pop.aip.org/authors>

## ADVERTISEMENT

The advertisement features the 'AIP Advances' logo in green and yellow, with a series of yellow circles of varying sizes to its right. Below the logo, the text 'Special Topic Section: PHYSICS OF CANCER' is displayed in white on a dark green background. Underneath, the phrase 'Why cancer? Why physics?' is written in yellow, and a blue button with the text 'View Articles Now' is positioned to the right.

AIP Advances

Special Topic Section:  
**PHYSICS OF CANCER**

Why cancer? Why physics? [View Articles Now](#)

## Aspect ratio effects on neoclassical tearing modes from comparison between DIII-D and National Spherical Torus Experiment

R. J. La Haye,<sup>1</sup> R. J. Buttery,<sup>1</sup> S. P. Gerhardt,<sup>2</sup> S. A. Sabbagh,<sup>3</sup> and D. P. Brennan<sup>4</sup>

<sup>1</sup>General Atomics, P.O. Box 85608, San Diego, California 92186-5608, USA

<sup>2</sup>Princeton Plasma Physics Laboratory, P.O. Box 451 Princeton, New Jersey 08543, USA

<sup>3</sup>Columbia University, 2960 Broadway, New York, New York 10027-6900, USA

<sup>4</sup>University of Tulsa, 800 South Tucker Drive, Tulsa, Oklahoma 74104, USA

(Received 7 November 2011; accepted 5 May 2012; published online 26 June 2012)

Neoclassical tearing mode islands are sustained by helically perturbed bootstrap currents arising at finite beta from toroidal effects that trap a fraction of the particles in non-circulating orbits. DIII-D and NSTX are here operated with similar shape and cross-sectional area but almost a factor of two difference in inverse aspect ratio  $a/R$ . In these experiments, destabilized  $n = 1$  tearing modes were self-stabilized (reached the “marginal point”) by reducing neutral-beam power and thus beta. The measure of the marginal island gives information on the small-island stabilizing physics that in part (with seeding) governs onset. The marginal island width on NSTX is found to be about three times the ion banana width and agrees with that measured in DIII-D, except for DIII-D modes closer to the magnetic axis, which are about two times the ion banana width. There is a balance of the helically perturbed bootstrap term with small island effects with the sum of the classical and curvature terms in the modified Rutherford equation for tearing-mode stability at the experimental marginal point. Empirical evaluation of this sum indicates that while the stabilizing effect of the curvature term is negligible in DIII-D, it is important in NSTX. The mode temporal behavior from the start of neutral-beam injection reduction also suggests that NSTX operates closer to marginal classical tearing stability; this explains why there is little hysteresis in beta between mode onset, saturation, and self-stabilization (while DIII-D has large hysteresis in beta). NIMROD code module component calculations based on DIII-D and NSTX reconstructed experimental equilibria are used to diagnose and confirm the relative importance of the stabilizing curvature effect, an advantage for low aspect ratio; the relatively greater curvature effect makes for less susceptibility to NTM onset even if the classical tearing stability index is near marginal. © 2012 American Institute of Physics. [<http://dx.doi.org/10.1063/1.4729658>]

### I. INTRODUCTION

Toroidicity in a tokamak makes the total magnetic field on a flux surface vary poloidally, so that it is stronger on the inboard side and weaker on the outboard side. When collisionality is low enough (as almost always in most tokamaks when ions make collisions at an effective rate smaller than the bounce frequency in trapped orbits), drift is added to particle gyrations and a fraction of particles are trapped on the outboard side in magnetic mirrors formed due to the poloidal variation of the magnetic field.<sup>1</sup> A bootstrap current arises (carried by passing electrons), which is approximately proportional to the product of the trapped fraction and the electron pressure gradient; this results from “friction” of passing electrons with trapped electrons and stationary ions and exists independently of inductively driven and neutral beam currents.<sup>2</sup> Neoclassical tearing modes (NTMs) are destabilized and sustained by helically perturbed bootstrap currents.<sup>3–6</sup> At sufficiently high beta (ratio of volume averaged plasma pressure to magnetic field pressure), a linearly stable tearing mode, if seeded by another MHD event, can have the seed reinforced, a destabilizing effect that can lower the plasma magnetic energy. However, curvature effects, i.e., field line bending by the island, tend to raise the magnetic energy, a stabilizing effect;<sup>7–11</sup> this is often called the

Glasser-Greene-Johnson (GGJ) effect after the original authors. The destabilizing helically perturbed bootstrap current is reduced, obviated, or weakened by a number of effects at small island size; this tends to make an NTM linearly stable and non-linearly unstable, i.e., metastable. Reference 6 reviews the literature, which includes cross-field transport,<sup>12–15</sup> ion polarization current,<sup>16–18</sup> and the reduction of the ion drive.<sup>19</sup>

All of the toroidal effects depend on how “spherical” a tokamak is. Here,  $R$  is the major radius of the plasma boundary surface about the magnetic axis and  $a$  is the minor radius. The closer  $R/a$  is to one, the greater the toroidal effects, and as  $R/a$  goes to infinity ( $a/R$  goes to zero), such effects cease to exist. While the GGJ effect is usually neglected at large aspect ratio (small inverse aspect ratio),<sup>6</sup> time dependent modeling in the low aspect ratio device MAST confirmed its significance at low aspect ratio.<sup>20,21</sup>

In this paper, experimental results are contrasted between the typical aspect ratio tokamak DIII-D ( $R/a = 2.7$ ) and the low aspect ratio NSTX ( $R/a = 1.4$ ). In Sec. II, the form of the modified Rutherford equation (MRE) for analysis is described both for lumped small island effects and with small island effects “broken out.” Section III has the experimental situations for DIII-D and NSTX with discussion of how the experiments are performed. The empirical scaling of

the marginal island width for self-stabilization (a key parameter that along with seeding governs onset) is given in Sec. IV along with some comparison to underlying mechanisms. Section V has the analysis of the balance at marginality of the destabilizing helically perturbed bootstrap current (with small island effects included) to the sum of the stabilizing classical tearing parameter (assumed stabilizing) and the curvature effect. Section VI describes calculations with full shaped geometry for DIII-D and NSTX equilibria utilizing the flux surface-averaging component module “fluxgrid” from the resistive MHD code NIMROD. This is used to check the empirical fits for the relative importance of the stabilizing curvature. Finally, a discussion is made in Sec. VIII.

## II. FORM OF THE MODIFIED RUTHERFORD EQUATION USED FOR EMPIRICAL ANALYSIS

For a  $q = m/n$  island of full width  $w$  at rational surface  $q$  of poloidal mode  $m$  and toroidal mode  $n$ , the island growth or decay<sup>4,6,20,22–36</sup> is here given by the MRE,

$$1.22^{-1} \frac{\tau_R}{r} \frac{dw}{dt} = \Delta' r + C_R \frac{r D_R}{w} + \varepsilon^{1/2} \frac{r L_q}{L_{pe}} \beta_{0e} \left[ \frac{1}{w} - \frac{w_{small}^2}{3w^3} \right]. \quad (2.1)$$

This form has all of the relevant stability terms, the classical tearing drive, the curvature stabilization, and the helically perturbed bootstrap destabilization, which is “turned off” at small island size. Here,  $\tau_R$  is a resistive time,  $r$  is the minor radius at  $q$  defined as  $(R_{out} - R_{in})/2$  on the midplane  $q$  surface [with  $R_o \equiv (R_{out} + R_{in})/2$ ],  $w$  (in meters) is taken at the outboard midplane location, and  $\Delta'$  (in  $m^{-1}$ ) is the effective non-linear classical tearing index in the presence of an island. Now,  $C_R r D_R/w$  is the GGJ effect of assumed good average magnetic field curvature with dimensionless  $D_R$  the “resistive interchange parameter.” To leading order in inverse aspect ratio  $\varepsilon = r/R_o$  at the rational surface,  $D_R \approx -(q^2 - 1)(L_q^2/r L_p) \beta$ , where  $L_q$  is the radial magnetic shear length  $q/(dq/dR)$  at the outboard midplane,  $L_p$  is the total pressure gradient scale length  $-p/(dp/dR)$  at the outboard midplane, and  $\beta = 2\mu_0 p/B_{T0}^2$  with  $p$  the local total pressure, and  $B_{T0}$  the toroidal field on axis.  $C_R = \mathcal{O}(1)$  is a constant of proportionality, which can be modified by finite aspect ratio effects. Other forms of the MRE, with or without the curvature term, make a guess at  $\Delta' r$  (something between 0 and  $-2m$ ) and fit a free constant proportional to the bootstrap current term. In Refs. 20 and 22–36 (in chronological order of publication), the choice (and number) of adjustable constants differs. This is in part due to which physics is included but largely from the uncertainty in computing  $\Delta'$  reliably from even the best reconstructed equilibria.<sup>37,38</sup> Here, the effective non-linear  $\Delta' r$  term is backed out from the balance of Eq. (2.1) at the marginal point, to be discussed; this neither relies on a guess nor on the sensitivity to calculation from an equilibrium reconstruction. Note that in Eq. (2.1) as throughout, experimental evaluation is at the outboard midplane  $q = m/n$  surface (where diagnostics tend to measure) and in general consists of ratios of two such locally evaluated quantities. The equivalent rigorous flux

surface averaged form of the MRE will be given in Sec. VI as Eq. (6.1); Eqs. (2.1) and (6.1) are of the same form with the same stabilizing and/or destabilizing terms.

The key parameter at issue is the local  $q = m/n$  surface inverse aspect ratio  $\varepsilon$ . This enters into the bootstrap drive, the GGJ curvature effect, and the small island stabilizing effects. For typical large aspect ratio tokamaks such as DIII-D,  $\varepsilon = r/R_o$ , but the physics actually comes from the dominant poloidal in/out asymmetry in  $B_T$ , which is itself only approximately  $r/R_o$ . Rigorously, toroidal effects come from the variation in total  $B$  of  $\varepsilon_B \equiv (B_{in} - B_{out})/(B_{in} + B_{out})$ .<sup>1</sup> For DIII-D as in the shape of Fig. 1,  $\varepsilon_B$  including both toroidal and poloidal field components from equilibrium reconstruction is only  $-0.3\%$  smaller than  $r/R_o$ . However, for NSTX as in the shape of Fig. 1,  $\varepsilon_B$  is  $14\%$  smaller than  $r/R_o$ . In this paper, for both devices,  $\varepsilon$  will always be evaluated from  $\varepsilon_B$ , not  $r/R_o$ , for each case, using the EFIT MHD equilibrium reconstruction that includes radial profiles of the local magnetic field pitch by the motional Stark effect (MSE) diagnostic. The sub B will now be dropped for convenience.

The destabilizing bootstrap current drive term in Eq. (2.1) is  $\varepsilon^{1/2}(r L_q/L_{pe} w) \beta_{0e}$  where  $L_{pe} = -p_e/(dp_e/dR)$  at the outboard midplane  $q = m/n$  and  $\beta_{0e} \equiv 2\mu_0 p_e/B_{\theta}^2$  is the local electron beta poloidal. Now this form for the bootstrap drive term is simplified for empirical analysis; the electron pressure is assumed to dominate the bootstrap current while it is known that different elements from electron density, electron temperature, and ion temperature gradients contribute.<sup>2</sup> Additionally, with a trapped fraction proportional to  $\sqrt{\varepsilon}$ , a better constant of

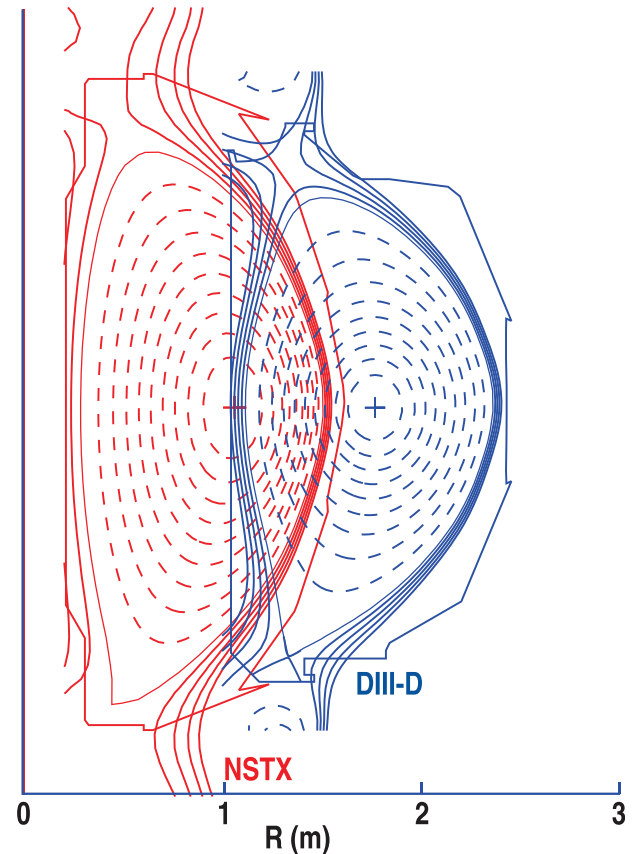


FIG. 1. Comparison of cross-sections of discharges run for these experiments in DIII-D and NSTX.

proportionality more valid for arbitrary aspect ratio occurs to leading order in  $\sqrt{\varepsilon}$  of  $[2.3\sqrt{\varepsilon}/(1 + 2.3\sqrt{\varepsilon})]$ .<sup>9</sup> We have simplified this as  $\sqrt{\varepsilon}$  in Eq. (2.1) for in the relevant range,  $\sqrt{\varepsilon} = 0.4 \sim 0.6$ , the bracket  $[2.3/(1 + 2.3\sqrt{\varepsilon})]$  is weakly varying near a value of one. Shaping effects and other choices for the bootstrap dependence on kinetics could be lumped into a “free” constant to be experimentally fitted.<sup>22</sup>

To leading order in  $\varepsilon$ , keeping the form in the bracket [] above, the ratio of the resistive interchange parameter<sup>8</sup>  $D_R \approx -(q^2 - 1)L_q^2\beta/rL_p$  to the simplified dimensionless neoclassical bootstrap drive<sup>9</sup>  $D_{nc} = [2.3\sqrt{\varepsilon}/(1 + 2.3\sqrt{\varepsilon})](L_q/L_{pe})\beta_{\theta e}$  is

$$\frac{D_R}{D_{nc}} \approx \frac{-(q^2 - 1)L_q^2\beta/rL_p}{2.3\sqrt{\varepsilon}(1 + 2.3\sqrt{\varepsilon})^{-1}L_q\beta_{\theta e}/L_{pe}}. \quad (2.2)$$

Note that both  $D_R$  and the  $D_{nc}$  terms in Eq. (2.1) scale as  $w^{-1}$  and thus this dependence cancels in the ratio Eq. (2.2). Both the numerator and denominator scale linearly with beta, but with different forms. As  $\beta/\beta_{\theta e} = (B_\theta/B_T)^2(1 + \frac{T_i}{T_e})$ , we can use  $q \approx \varepsilon(B_T/B_\theta)(1 + \kappa^2)/2$  with  $T_i \approx T_e$  and  $L_p \approx L_{pe}$  to get a ratio from Eq. (2.2) based on geometry only; here,  $\kappa$  is the elongation of the rational surface and we neglect flux surface triangularity as yet a higher order effect,

$$\frac{D_R}{D_{nc}} \approx \frac{-(q^2 - 1)}{q^2} \left(\frac{L_q}{r}\right) \frac{(1 + \kappa^2)^2}{4.6} \varepsilon^{1/2}(1 + 2.3\sqrt{\varepsilon}). \quad (2.3)$$

This scales as  $\varepsilon^{3/2}$  for  $2.3\sqrt{\varepsilon} \ll 1$ , which is often assumed, but not rigorous and becomes proportional to  $\varepsilon^2$  for  $2.3\sqrt{\varepsilon} > 1$ . For evaluation at the rational surface  $q = 2$ ,  $L_q/r \approx 1/2$ , and  $\kappa \approx \sqrt{3}$ ,  $D_R/D_{nc} \approx -1.3 \varepsilon^{3/2}(1 + 2.3\sqrt{\varepsilon})$ , which is relatively small ( $\approx -0.2$ ) for  $\varepsilon = 1/5$  (DIII-D) and significant ( $\approx -0.6$ ), for  $\varepsilon = 1/3$  (NSTX).

Finally, all of the small island stabilizing effects are lumped together as  $w_{small}$ . The bracket has the limit of  $w^{-1}$  for large island widths, so that only the primary destabilizing helically perturbed bootstrap current effect is retained. The factor 3 in the Eq. (2.1) bracket allows for the bootstrap term *with* the small island effects to be maximum at  $w = w_{small}$ , i.e., the destabilizing term *decreases* with smaller island width. Experimental situations are to be described in which a “marginal” condition is accessed in which the metastable space ( $dw/dt > 0$  for some finite range in  $w$ ) is just removed. The “broken out” form (times  $w$ ) of the bracket in Eq. (2.1) with the individual small island physics effects (all of which co-exist) is

$$\left[1 - \frac{w_{small}^2}{3w^2}\right] = \left[\frac{\delta w^2}{w^2 + 28w_{bi}^2} + \frac{w^2}{w^2 + w_d^2} - \frac{w_{pol}^2}{3w^2}\right]. \quad (2.4)$$

The first effect in the right-hand side represents the reduction of the “ion drive,” which contributes  $\delta$  in addition to the electron drive [ $\delta \approx 2/3$  for example, if  $T_i \approx T_e$  and  $\nabla T_i \approx \nabla T_e$ , flat  $n_e$ , per Refs. 2, 19, and 33]. Here,  $w_{bi} = \varepsilon^{1/2}\rho_{\theta i}$  is the ion banana width with  $\rho_{\theta i} = (2m_i k_b T_i / e^2 B_\theta^2)^{1/2}$  the poloidal ion gyroradius. For  $w \lesssim w_{bi}$ , the assumption of islands larger than the ion banana width breaks down and the factor 28 is from an analytic (numerical) fit to account for this.<sup>19</sup> For marginal island widths of

$2 \sim 3 w_{bi}$  (as in these experiments to be presented later), the analytic factor 28 makes for a reduction of  $\delta$  to  $1/8 \sim 1/4$  of its large island value; this suggests that the contribution of the ions to the bootstrap drive can indeed be neglected as the effective  $\delta$  becomes  $\ll 1$ . Only large islands with  $w > \sqrt{28}w_{bi}$  would have this contribution in effect, something which could be combined with the Sauter coefficients for the equilibrium based analysis in future work.

The electron transport threshold in Eq. (2.4) is characterized by a width  $w_d$  within which transport perpendicular to  $w$  can wash out the electron drive;<sup>12–15</sup> however, note that while  $w_d = \Theta(\varepsilon^{1/2}\rho_{\theta i})$ , it does not scale with  $\varepsilon^{1/2}\rho_{\theta i}$ . The form with  $w_d$  in Eq. (2.4),  $w^2/(w^2 + w_d^2)$  has a “soft” gradual turn off with increasing  $w$ . For marginal islands in this work found to have  $w^2$  much larger than estimates of  $w_d^2$ , one can expand, so that  $w^2/(w^2 + w_d^2) \approx 1 - w_d^2/w^2$ . Effectively,  $3w_d^2$  is added in practice to  $w_{pol}^2$  in Eq. (2.4), so that  $w_{small}^2 \approx w_{pol}^2 + 3w_d^2$  includes both transport and ion polarization current effects (discussed next) with the  $\delta$  term taken as  $\ll 1$  (previously discussed).

Finally, the last term in the RHS of Eq. (2.4) is from ion polarization currents, which arise because of inertial effects in an island and are stabilizing for island propagation (in the plasma frame of flow) between zero and the ion diamagnetic drift frequency.<sup>16–18</sup> The theory of the effect of the induced helical polarization current by the island on the island itself has evolved considerably as discussed in Sec. III E of Ref. 6. The characteristic island to represent the strength of this effect is given by  $w_{pol} \approx (0 \sim 3)\varepsilon^{1/2}\rho_{\theta i}$  depending on the island flow magnitude and sign and on collisionality.

All of these three small island effects in Eq. (2.4) can co-exist and be cumulative and are hard to sort out. The lumped form on the LHS in Eq. (2.4) has the advantage of a “harder” break in  $dw/dt$  as beta and  $w$  are reduced, to be discussed, than that of a form  $w^2/(w^2 + w_{small}^2)$ ; this was contrasted previously in Refs. 20 and 25 for example.

### III. EXPERIMENTS IN DIII-D AND NSTX

The experimental procedure in each device is: (1) raise beta in a high confinement H-mode to excite an  $m/n = 2/1$  mode, (2) “slowly” reduce neutral beam injection (NBI) power and thus beta, (3) stay in H-mode as power is reduced, (4) avoid the rotating  $n = 1$  mode locking to the resistive wall as torque is reduced with less NBI, and (5) reach the marginal point for self-stabilization, i.e., removal of the metastable parameter space. DIII-D and NSTX cross-sections are shown in Fig. 1. By comparing NTM behavior in these devices, the effects of aspect ratio over a range of almost two can be studied. Both devices are run with near balanced double null divertor shapes of similar minor radius ( $a \approx 0.60$  m), elongation ( $\kappa \approx 2$ ) triangularity ( $\delta_u \approx 0.4$  and  $\delta_\ell \approx 0.7$ ) and cross sectional area ( $\approx 2$  m<sup>2</sup>).

#### A. DIII-D

DIII D was run with plasma current  $I_p = 0.8$  MA and axial toroidal field  $B_{T0} = 1.3$  or 2.0 T, so as to vary the safety factor at the 95% flux surface from  $q_{95} = 4.3$  to 6.9. The plasma current in DIII-D was chosen at a lower than usual

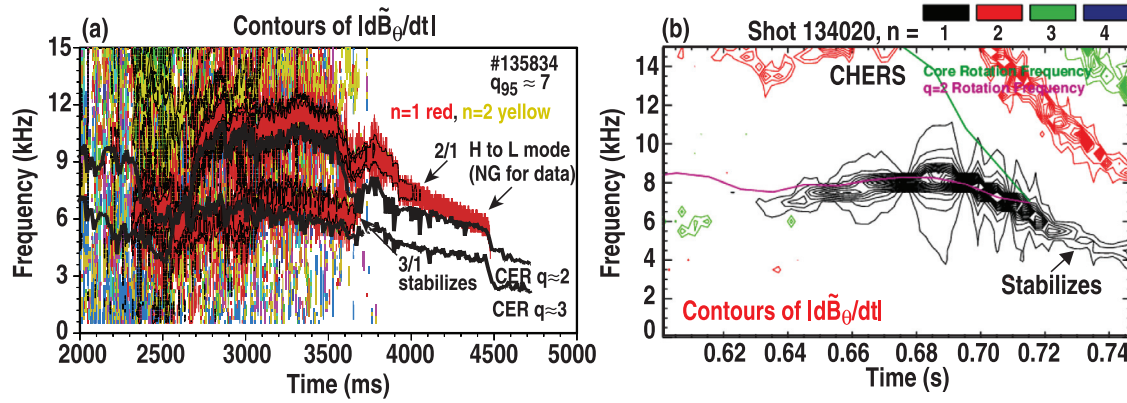


FIG. 2. (a) Spectrogram of Mirnov activity  $|d\tilde{B}_\theta/dt|$  contours versus time for DIII-D at the higher  $q_{95}$  in which both  $m = 3/1$  and  $2/1$  modes were excited. As beta is ramped down (not shown), the initially locked modes break free, the  $3/1$  mode stabilizes, and then the  $2/1$  mode stabilizes (but after an  $H \rightarrow L$  transition so the  $2/1$  marginal island data are not used.) CER measures of CVI toroidal rotation at chords closest to  $q = 2$  and  $3$  are superimposed. (b) Same for NSTX with  $2/1$  mode only and superimposed CHERS rotation both on axis and fitted to the  $q = 2$  location from MSE EFIT; the  $q = 2$  CHERS rotation is close to the  $n = 1$  Mirnov frequency.

value to be close to that of NSTX and to have similar  $q_{95}$  as at the standard 2.0 T value of DIII-D toroidal field. The lower 1.3 T value of DIII-D  $B_{T0}$  was also run to allow examination of the conditions at the usual lower  $q_{95} \approx 4$  DIII-D operation. DIII-D had to use gas puffing to stay in H-mode, otherwise, an H to L transition occurred and beta rapidly collapsed and profiles changed quickly. Spectrograms for Mirnov modes showing onset, decay, and stabilization are given in Fig. 2(a) for DIII-D.

DIII-D exhibits large hysteresis in beta between  $n = 1$  NTM excitation and the marginal point for self-stabilization. This is shown in Fig. 3 for a discharge in which only the  $m/n = 2/1$  mode is excited (the excitation of an NTM metastable state by a seed island is discussed in Sec. V). A signature of an NTM is that the Mirnov amplitude  $|\tilde{B}_\theta|$  measured by an outboard midplane wall array is proportional to the square of global  $\beta_\theta$  for large island width and profiles nearly constant. Thus, a multiplier of  $\beta_\theta^2$  is plotted versus time to exactly overlay at the start of the NBI rampdown. These track well together until deviation comes after 3.0 s (small

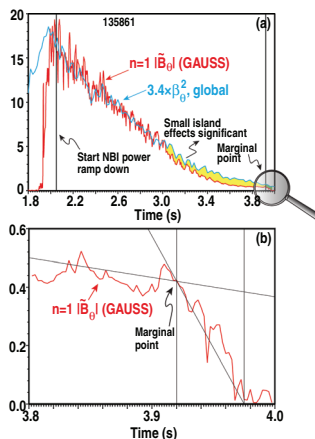


FIG. 3. (a)  $3.4 \times \beta_\theta^2$  and  $n = 1 |\tilde{B}_\theta|$  in DIII-D versus time for a single  $m/n = 2/1$  excited mode. The start of the NBI power rampdown is noted, which lowers the global  $\beta_\theta$ . (b) Blowup of  $|\tilde{B}_\theta|$  vs.  $t$  in the self-stabilization. The marginal point is noted.

island effects become significant) and stabilization starts at the marginal point (small island effects dominate). The self-stabilization period is blown up in Fig. 3(b). The transition from a slowly decaying  $n = 1$  Mirnov amplitude to a rapid decay, to complete stability is fairly sharp.

The analysis in Secs. IV and V relies on measuring the full width of the marginal island on the outboard midplane. In DIII-D, this is evaluated from the external poloidal magnetic field probe (Mirnov) toroidal array and the MSE EFIT with a calibration for the geometry (shaping, toroidicity, etc.) by benchmarking to the radial profile of electron cyclotron emission (ECE) at the mode frequency; this is done for “fat” saturated islands before NBI ramp-down to get better resolution.<sup>29</sup> Islands “short circuit” the pressure (as well as  $n_e$ ,  $T_e$ , and  $T_i$ ) gradients across the island unless cross-field transport dominates and washes out this effect. As a result, flat spots (no gradients) appear across the island O-points; this results in the characteristic  $T_e$  radial perturbation for direct island width measure. However, ECE radial resolution is too coarse for small island width accuracy. Thus, one calibrates large island width magnetics by ECE to determine small island widths by magnetics. The perturbed radial field  $|\tilde{B}_r|$  at  $q = m/n$  is found from  $|\tilde{B}_r| \approx 0.5 |\tilde{B}_\theta| [(R_{\text{Mirnov}} - R_o)/r]^{m+1}$  where  $R_{\text{Mirnov}}$  is the major radius of the magnetic probe array. The island width is found from  $w \approx C_{\text{ECE}} (16L_q R_o |\tilde{B}_r| / n B_{T0})^{1/2}$ . There are three separate cases in DIII-D:  $m/n = 2/1$  in discharges with  $q_{95} = 4.3$ ,  $m/n = 3/1$  with  $q_{95} = 7.2$ , and  $m/n = 2/1$  with  $q_{95} = 6.9$ . The separate systematic correction factors with uncertainty due to ECE channel spacing are found to be  $C_{\text{ECE}} = 0.67 \pm 0.24$ ,  $0.68 \pm 0.21$ , and  $0.74 \pm 0.19$ , respectively. They apply equally to each separate case, i.e., are a constant equally multiplying each analyzed island width. These factors are used to get  $w_{\text{marg}}$  down to  $\lesssim 2$  cm where ECE channel spacing would make determination much more uncertain.

## B. NSTX

The NSTX parameters are standard for reliable H-mode operation. NSTX has  $I_p = 0.9$  MA and  $B_{T0} = 0.44$  T for

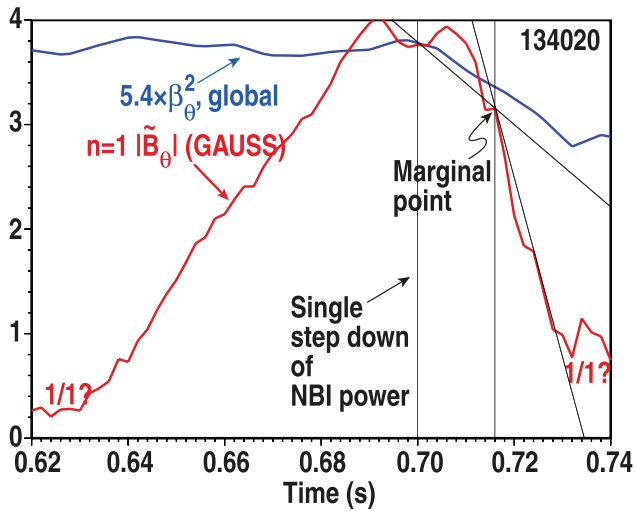


FIG. 4. Same as Fig. 3 but for the NSTX  $m/n = 2/1$  mode. The multiplier on  $\beta_\theta^2$  global is adjusted to match  $n = 1 |\tilde{B}_\theta|$  at the start of NBI reduction.

$q_{95} = 8.0$ . NSTX developed a reproducible  $n = 1$  onset condition using modest  $Li$  evaporation and mode locking was avoided by using both  $n = 1$  and  $n = 3$  error field correction (DIII-D used just standard  $n = 1$  error field correction). Spectrograms for Mirnov modes showing onset, decay, and stabilization are given in Fig. 2(b) for NSTX. NSTX exhibits little hysteresis between  $n = 1$  NTM excitation (discussed in Sec. V) and the marginal point for self-stabilization. This is shown in Fig. 4 for the  $m/n = 2/1$  mode, which saturates and is here closely followed by a single step down of NBI power (to  $2/3$  the initial value); the mode wanes somewhat, then stabilizes. NSTX, without ECE, has the best radial resolution from  $T_i$  measurement. Here, NSTX has just the  $m/n = 2/1$  case with  $q_{95} = 8.0$ . The “fat” island flat spot in  $T_i$  is evaluated from the CHERS (charge exchange recombination spectroscopy and charge exchange recombination (CER) in DIII-D) diagnostic of the radial profile of impurity ion temperature, which has better radial spatial resolution than that of the Thomson diagnostic of the  $T_e$  profile; Thomson measured  $n_e$  profile being flat in H-mode is even less useful. The island widths  $w_{sat}$  for each discharge in NSTX are evaluated from  $T_i$  flat spots and scaled modestly down to the marginal point (as there is little hysteresis) to  $w_{marg} = w_{sat} (\tilde{B}_{\theta,marg}/\tilde{B}_{\theta,sat})^{1/2}$  as EFITs indicate little change in  $q$  profiles during the modest decrease in beta from saturation to marginality. The CHERS spacing sets an estimated uncertainty in the coefficient of proportionality of  $\pm 23\%$ , which is somewhat less than the relative uncertainty in DIII-D by ECE channel spacing. Note also that in NSTX, the estimated uncertainty in island width is not a systematic factor.

#### IV. MARGINAL ISLAND WIDTH SCALING

An NTM stabilizes when  $dw/dt = 0$  at  $w = w_{marg}$  and  $dw/dt < 0$  for all other  $w$ ; the metastable parameter space is removed at slightly lower beta and the mode is then completely stable. The measure of the marginal island width gives information on the small island stabilizing physics, that in part, along with the seed island physics, governs

onset. If the effective  $w_{small}$  is larger, an NTM is harder to excite, i.e., requires a larger seed from another MHD event, or needs beta to be raised to expand the  $dw/dt > 0$  space making seeding easier. Once the NTM is excited and sustained by a balance of effects, the marginal point gives a measure of small island effects without the complications from mixing in seeding. In this paper, we want to measure how the small island effects depend on aspect ratio.

#### A. DIII-D

The marginal island width for  $m/n = 3/2$  modes in typical “high” aspect ratio tokamaks was previously found to be about twice the ion banana width in a multi-machine (ASDEX Upgrade, DIII-D, JET, and JT-60U)  $q_{95} \approx 4 \sim 5$  database.<sup>32</sup> The factor two was consistent with cases using either beta rampdown (in Ref. 25) or with beta maintained at a high level, but electron cyclotron current drive (ECCD) at  $q = 3/2$  used to shrink the island width to reach marginality. The DIII-D  $m/n = 3/2$  data with beta rampdown (not with ECCD) are now reanalyzed for this paper. This allows putting the previously published  $n = 2$  DIII-D data in context with that from NSTX and DIII-D for  $n = 1$  modes. The DIII-D shaping used for Ref. 32 compared to that in this DIII-D/NSTX paper was with lower  $R/a = 3.2$ , a little higher  $q_{95} = 4.6$ , and  $C_{ECE} = 0.71 \pm 0.18$ . The reanalyzed DIII-D  $3/2$  data of  $w_{marg}$  are well correlated with  $(2.4 \pm 0.3)\epsilon^{1/2}\rho_{\theta i}$  with linear correlation  $r = 0.75$  whether the fit is forced through zero at the origin or not. Note that the EFIT is used to locate  $q$  and the outboard midplane value of  $B_\theta$  there (as well as the values of  $B_\theta$  and  $B_T$  both inboard and outboard for  $\epsilon$ ); CER is used to get  $T_i$  at the  $q$ -location. The one sigma fitting uncertainty (only 40% of the systematic uncertainty) puts the lower range of the ratio at just above 2 for DIII-D data only. The empirical factor of 2 for the multi-device high aspect ratio  $m/n = 3/2$  marginal island is what we want to compare to in the present DIII-D/NSTX paper.

The new  $n = 1$  data from DIII-D for full marginal island width at the outboard midplane versus ion banana width is shown in Fig. 5. The three separate  $n = 1$  DIII-D cases do not individually have enough data to separately correlate.

#### B. NSTX

The NSTX data for full marginal island width at the outboard midplane versus ion banana width are also shown in Fig. 5. The NSTX data alone have a ratio of  $3.0 \pm 0.4$  of the ion banana width whether forced through zero at the origin or not with a nice linear correlation of 0.88. The one sigma fitting uncertainty is about 60% of the uncertainty estimated from CHERS spacing (which is not systematic).

#### C. Comparison of DIII-D to NSTX

Two of the three  $n = 1$  DIII-D cases in Figure 5 overlap the NSTX data, while a third case in which  $q = 2/1$  is closer to the magnetic axis, has a lower ratio of  $1.8 \pm 0.1$  for the three data points. Error bars for an NSTX case and two different  $2/1$  DIII-D cases to be analyzed in more detail later in this paper are included in Fig. 5. The ratio of the marginal

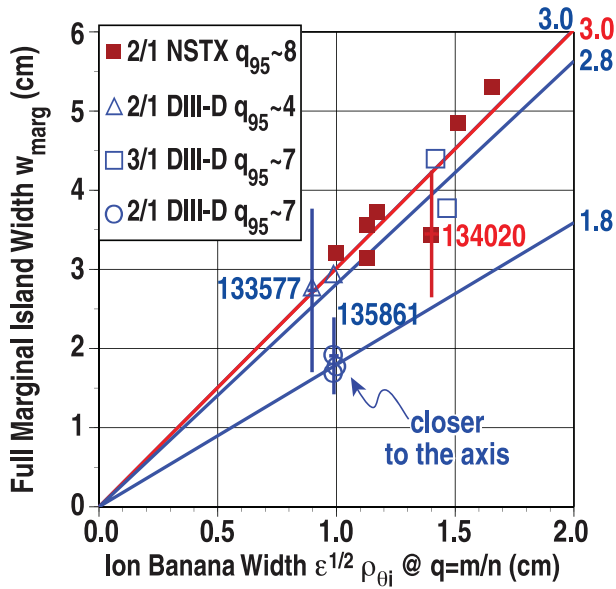


FIG. 5. Full marginal island width at outboard midplane  $q = m/n$  versus local ion banana width. NSTX and two of three DIII-D cases have a ratio of about 3 while the one of three DIII-D cases that is closer to the magnetic axis (smaller local inverse aspect ratio magnetic field variation) is closer to a ratio of 2.

island width to the ion banana width is well correlated with  $\varepsilon^{1/2}$  as shown in Fig. 6. However, the range in  $\varepsilon^{1/2}$  is only from 0.4 to 0.6. Error bars for the three study cases are again included. That the empirical  $m = 2$  or  $3$ ,  $n = 1$  marginal island width with respect to the ion banana width increases with inverse aspect ratio from  $\approx 2$  to  $\approx 3$  is consistent with the previous high aspect ratio  $m = 3$  and  $n = 2$  scaling value.

### D. Comparison of experiment with theory

The two physics mechanisms which could be the source of the marginal islands observed are that from cross-field transport “washing out” the helically perturbed bootstrap current drive and/or the stabilizing island-induced helical polarization currents due to finite island flow in the plasma frame.

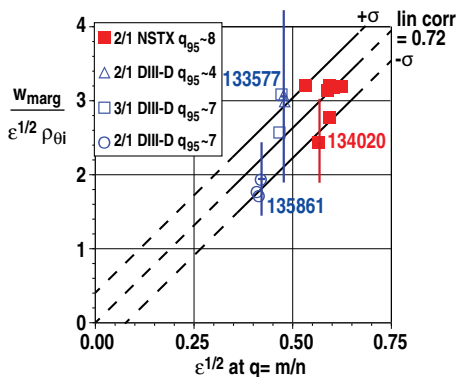


FIG. 6. Ratio of the marginal island width to the ion banana width versus square root of the “inverse aspect ratio” (from total B). The linear correlation is 0.72 and the one sigma uncertainties in the fit are added.

TABLE I. Evaluation of sources of small island effects at the marginal point for  $m/n = 2/1$ .

|  | NSTX #134020    | DIII-D #133577   | DIII-D #135861   |
|--|-----------------|------------------|------------------|
| $\varepsilon^{1/2}$                          | 0.567           | 0.478            | 0.402            |
| $w_{marg}$ (cm)                              | 3.42            | 2.76             | 1.71             |
| $w_{bi} = \varepsilon^{1/2} \rho_{\theta i}$ | 1.40            | 0.89             | 0.99             |
| $w_d$ (cm)                                   | 1.07            | 1.03             | 0.82             |
| $(v_i/\varepsilon)/ \omega_e^* $             | 0.84            | 2.73             | 1.09             |
| $\omega/\omega_i^*$                          | $0.23 \pm 0.37$ | $-0.20 \pm 0.38$ | $-0.07 \pm 0.30$ |
| $(3L_q/L_{pe})^{1/2} w_{bi}$                 | 3.01            | $1.52 (4.60)^a$  | 2.16             |

<sup>a</sup>High collisionality is enhanced by  $\varepsilon^{-3/4}$ .

Detailed evaluation of selected  $m/n = 2/1$  cases from both high and low  $q_{95}$  DIII-D and from NSTX has been carried out as to the dominant (if any) effect in  $w_{marg}$ ; these are the same three cases analyzed by NIMROD to be discussed in Sec. VI. These cases are 134020 for NSTX as in Fig. 4, 133577 for DIII-D, and 135861 for DIII-D as in Fig. 3. The values of  $\varepsilon^{1/2}$  at  $q = 2$  are 0.567, 0.478, and 0.402, respectively. Parameters are given in Table I.

Using cross-field transport  $\chi_{\perp}$  as gyroBohm and collisional parallel ion transport  $\chi_{\parallel}$ , the values of  $w_d$  are too small to account for  $w_{marg}$ . The characteristic island size<sup>12–15</sup> is  $w_d \approx (L_s/k_{\theta})^{1/2}/(\chi_{\perp}/\chi_{\parallel})^{1/4}$  with  $L_s = qL_q/\varepsilon$  the parallel magnetic shear length,  $k_{\theta} = m/r$  the poloidal wave number, and  $\chi_{\perp} \approx \nu_i \rho_{\theta i}^2$  the gyroBohm cross-field transport<sup>39</sup> with  $\nu_i$  the ion collisionality [ $\nu_i = 5.09 \times 10^{-7} n_e (cm^{-3}) T_i (eV)^{-3/2}$ ]. If the ion mean free path  $\lambda_i = V_i/\nu_i$ , [ $V_i = (2k_B T_i/m_i)^{1/2}$ ] is less than the parallel island correlation length  $\lambda_{\parallel} = 4\pi L_s/k_{\theta} w_{marg}$ , then  $\chi_{\parallel} \approx V_i^2/\nu_i$ . Note that one must say here that the entire “ $w_d$ ” theory breaks down for island widths which are not many radial step sizes ( $\approx \rho_{\theta i}$  for gyroBohm) for cross-field diffusive transport; this is a theoretical issue that needs to be addressed.

The characteristic ion polarization island width  $w_{pol}$  scales naturally as  $\varepsilon^{1/2} \rho_{\theta i}$  but depends on both the collisionality regime<sup>16–18</sup> [ $(\nu_i/\varepsilon)/\omega$ ], and the net island rotation  $\omega$  in the frame rotating with the plasma. Here, the normalized collisionality is the ratio of the ion collision frequency (divided by the trapped ion fraction) to  $\omega$ , and  $\omega$  is evaluated with respect to  $\omega_i^*$  the ion diamagnetic drift frequency in the  $E_r \times B = 0$  frame of the rotating plasma.<sup>18</sup> The diamagnetic drift frequency for species  $j$  is  $\omega_j = nk_B T_j (dp_j/d\psi/e_j p_j)$  where the gradient  $p_j$  is with respect to the poloidal flux (profile from EFIT). With  $|\omega_e^*|$ , the magnitude of the electron diamagnetic drift frequency, the values of  $(\nu_i/\varepsilon)/|\omega_e^*|$  for the cases analyzed cluster around unity as given in Table I. Values of  $|\omega_e^*|$  instead of  $\omega$  are used for evaluating collisionality as the values of  $\omega/\omega_i^*$  (with error bars) cluster around zero; a zero value implies no ion polarization current, as there is no island rotation in the plasma frame and so no polarization current is induced. An effective  $w_{pol}$  only occurs theoretically for values of  $\omega/\omega_i^*$  between 0 and 1. Negative values are problematic as theory “breaks down.” Previous DIII-D evaluations found  $\omega/\omega_i^* = \mathcal{O}(1)$  at low collisionality.<sup>18</sup> Here as in Ref. 18, MSE EFIT is used to find the location of  $q = 2$ . CER or CHERS is used to get the

plasma frame  $E_r \times B$  rotation from toroidal rotation corrected by the  $\nabla p_i$  term (a small effect) but the poloidal rotation is taken as zero [due to strong poloidal flow damping, particularly in NSTX, but indeed a very small effect in Ref. 18 where it was included]. Taking the low collisionality regime [ $(\nu_i/\varepsilon)/|\omega_e^*| \ll 1$ ] and evaluating for an assumed stabilizing island flow,  $w_{pol} \approx (3L_q/L_{pe})^{1/2} w_{bi}$  and is given in Table I. The first and third cases have reasonable agreement with  $w_{marg}$ , but the second case with both higher collisionality and possibly negative propagation does not. Allowing for a higher collisionality regime theoretically enhances  $w_{pol}$  by  $\varepsilon^{-3/4}$ .<sup>16,18</sup> This is also given in Table I for case 2 which has a collisionality higher than unity. The measured value of  $w_{marg}$  falls between the low and high collisionality values. However, it is again noted that rotation is (within error bars) close to zero or somewhat negative, which should theoretically negate the ion polarization current effect.

A theoretically consistent explanation of the empirical marginal island scaling remains elusive. The transport model, even if theoretical inconsistencies are neglected, does not yield large enough values or have the correct scaling with ion banana width. The polarization model is consistent with the size, scaling, and effect of collisionality but island flow in the plasma frame is measured to be inconsistent with a stabilizing effect. When the curvature and bootstrap terms are comparable, as at low aspect ratio for example, the measure of  $w_{marg}$  is not necessarily  $w_{small}$ . This is addressed later in evaluating the MRE from excitation of an island, to saturation, to the marginal point where stabilization occurs.

## V. MRE BALANCE AS A METHOD TO EVALUATE THE IMPORTANCE OF THE CURVATURE EFFECT

The DIII-D and NSTX cases at the marginal point are balanced with the destabilizing helically perturbed bootstrap current (including the small island effects lumped together as  $w_{small}$  in Eq. (2.1)) just cancelled by the stabilizing sum of the classical tearing parameter (assumed stabilizing, i.e., negative, and possibly non-linear, i.e., having a dependence on  $w$ ) and by the good magnetic field curvature term (the GGJ effect). In this section, we wish to evaluate the relative importance of the curvature term with aspect ratio. The form of Eq. (2.1) with  $1.22^{-1} \tau_R(dw/dt)/r \equiv 0$  is used here, while we follow up in Sec. VI with the equivalent  $k_o(dw/dt)/\eta^* \equiv 0$  of Eq. (6.1) for full shaped geometry. Any situation in which an island width is stationary in time, is, i.e., “saturated” or slowly evolving [so that  $1.22^{-1} \tau_R(dw/dt)/r$  on the LHS of Eq. (2.1) is “small”] could be used to evaluate terms in this balance. This work makes use of the slow (NSTX) or very slow (DIII-D) decrease of island widths leading to the marginal point and self-stabilization. As a check, the NSTX case #134020 of Fig. 4 is evaluated as to how big  $1.22^{-1}(\tau_R/r)dw/dt$  is. The resistive diffusion of flux within the  $q = m/n$  surface is  $\tau_R \approx \mu_o Z_{eff}^{-1} f(\varepsilon) \sigma_{sp} T_e^{3/2} r^2$  with  $\mu_o = 4\pi \times 10^{-7}$  the permeability of free space,  $\sigma_{sp}$  the Spitzer conductivity coefficient [explicitly calling out the  $Z_{eff}$  and trapped electron correction  $f(\varepsilon)$  dependencies],<sup>1,40,41</sup> and  $r$  the minor radius of the flux surface as previously described.

The effect of electron trapping reduces conductivity by a factor  $f(\varepsilon) \approx (1 - 1.80\sqrt{\varepsilon} + 0.80\varepsilon)^{-1}$ , which is here  $\approx 0.21$ .<sup>42</sup> Using  $\sigma_{sp} = 1278(sm^{-1}H^{-1}eV^{-3/2})$ ,  $T_e = 429$  eV,  $r = 0.356$  m, and  $Z_{eff} = 2$  with  $f(\varepsilon) = 0.21$  yields  $1.22^{-1} \tau_R(dw/dt)/r \approx -0.09$  (with  $\tau_R = 0.21$  s), which is indeed “slow” and small compared to the bootstrap term in the RHS of Eq. (2.1) evaluated from measured quantities (which is discussed next). Note that the first use of this  $\tau_R$  in the MRE for evolution of an NTM was made in TFTR taking an older simpler (but comparably quantitative) model of the neoclassical resistivity correction.<sup>43</sup>

All DIII-D and NSTX cases are evaluated at the marginal point using Eq. (2.1) with the bracket set to  $2/(3w_{marg})$ . This assumes that the variations with  $w$  in  $\Delta'r$  and with  $w$  in the curvature term  $\propto w^{-1}$  are both small with respect to the bootstrap term  $\propto w^{-1}$ . This is justifiable for  $\Delta'r \approx C_o - C_1 w$  (with  $C_o$  and  $C_1$  constants) at small island sizes and at high aspect ratio if the curvature term is relatively small compared to the bootstrap term. In this case, the most unstable  $w$  is at  $w_{marg} \approx w_{small}$ .

The inferred sum of the  $\Delta'r$  and curvature terms versus safety factor  $q_{95}$  is shown in Fig. 7. Error bars are for the three study cases previously mentioned. These error bars are predominantly from evaluating island width and from fitting the electron pressure gradient scale length.) The  $m/n = 2/1$  mode in DIII-D shows greater classical stability at larger  $q_{95}$ . This is unsurprising as low beta experiments at lower  $q_{95}$  much below 3 inevitably induce 2/1 tearing as current profiles become unstable.<sup>44</sup> However, surprisingly, the  $m/n = 3/1$  mode in DIII-D is interpreted to be less classically stable at its marginal point than the 2/1 mode at its marginal point at the same high  $q_{95}$ . As seen in Fig. 2(a), the differentially rotating (from 2/1) 3/1 mode stabilizes earlier in the beta rampdown. If one expects  $-\Delta'r$  to be of order 2 m or less,<sup>38</sup>

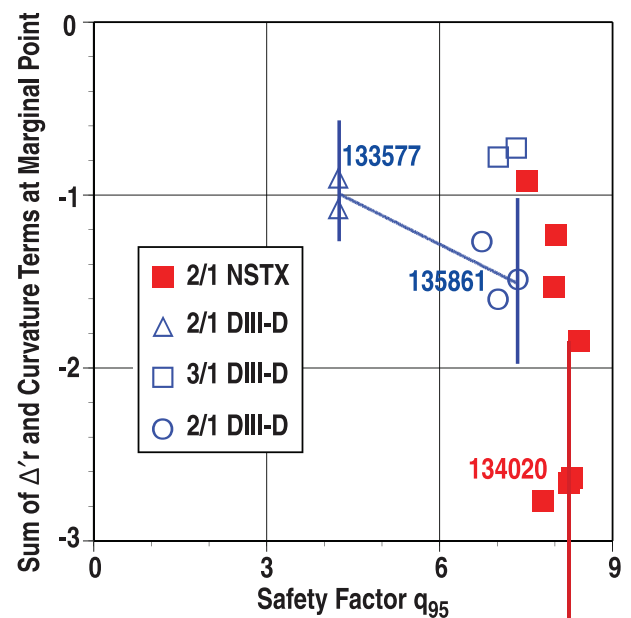


FIG. 7. Sum of the  $\Delta'r$  and GGJ terms (from balance with the helically perturbed bootstrap term evaluated at the marginal point) versus safety factor  $q_{95}$ .

the  $m = 3$  mode would be classically more stable. However, in Fig. 2(a), one can see that it is stabilized while the  $m = 2$  mode at the same time and beta remains non-linearly destabilized. A principal difference between the early 3/1 stabilization and the late 2/1 stabilization (both at  $q_{95} \approx 7$  ELMing H-mode) is the 2.5 times higher beta at the earlier 3/1 marginal time.

In contrast to DIII-D, the NSTX 2/1 data at the marginal point, all at about the same  $q_{95}$ , show a wide variation in Fig. 7. A hidden variable is clearly indicated. We look for this in plotting the inferred sum of the  $\Delta'r$  and curvature terms from the MRE balance versus the variation of the form of the curvature term alone in Fig. 8, where the curvature term on the horizontal axis is calculated from EFIT equilibria and the CER/CHERS and Thomson data. Error bars are again noted for the three study cases with the curvature term uncertainty dominated by both evaluating island width and the fitting of the total pressure gradient scale length. There is a good correlation for NSTX with the computed curvature parameter  $rD_R/w$  with linear correlation of 0.88. The uncertainty of the multiple data point fit is about half of the uncertainty estimated for a single data point. Again, lacking a reliable independent calculation (or measure) of the non-linear  $\Delta'r$  term, one cannot subtract it from the sum to get a residual alone that constitutes the curvature term, which in turn, could be compared to theory. However, this NSTX linear fit does give us two fitted numbers which, if  $\Delta'r$  and  $C_R$  are the same for all the data points allow us to back out both values. The linear fit (not forced through zero) extrapolates to about 0 at  $rD_R/w = 0$ . This suggests that  $\Delta'r \approx 0.0 \pm 0.4$  to the one

sigma of the fit and that the curvature term with  $C_R \approx 1.0 \pm 0.13$  is thus the dominant stabilizing effect that balances the helically perturbed bootstrap term (with small island effects). This explains the relatively small hysteresis in beta in NSTX between the saturated balance before NBI stepdown and the marginal point shortly after stepdown; if the curvature term  $\propto \beta$  and the bootstrap term  $\propto \beta_{\theta e}$  scale together and are delicately balanced, with  $\Delta'r$  “small,” there is little difference between these two operating points. In contrast to NSTX, the curvature parameter in DIII-D for all three cases is much smaller as also seen in Fig. 8. Thus, the stabilizing term in DIII-D is dominated by negative  $\Delta'r$  and a large hysteresis in beta occurs.

The MRE fit for DIII-D is shown in Fig. 9 for the  $m/n = 2/1$  case #135861. The marginal data point is fitted with the curvature neglected and labeled global  $\beta_{\theta} = 0.45$ . As  $\dot{w} = 0$ , the Y-axis value is 0, independent of the value of  $\tau_R$  estimated. Then using the same  $\Delta'r$  and profiles, the marginal point is projected back in time to the start of the NBI ramp down which has  $\beta_{\theta} = 2.22$  (and  $w_{small} \propto T_i^{1/2} \propto \beta_{\theta}^{1/2}$  is increased). Again, as  $\dot{w} = 0$ , the Y-axis value is 0 independent of  $\tau_R$ . There is good agreement between the measured high beta saturated island and the value estimated from the zero crossing of the high beta curve (11.6 vs. 12.2 cm) in Fig. 9. Finally, it is noted that an  $m/n = 1/1$  fishbone chirping down in frequency (with  $m \pm 1 = 1 \pm 1$  including  $m = 2$  sideband) is the seed (at a value of  $\beta_{\theta} = 2.24$ ) that grows to saturation. This point ( $w \approx 5.9$  cm measured at 160 cm/s) is added in Figure 9 to the MRE curve for high beta and is consistent with the MRE fit for  $\tau_R \approx 0.35$  s. The resulting calculated value of  $\tau_R \approx \mu_0 Z_{eff}^{-1} f(\epsilon) \sigma_{sp} T_e^{3/2} r^2$  from resistive diffusion within the island rational surface for  $Z_{eff} = 2$ ,  $T_e = 2450$  eV, and  $r = 0.30$  m, is about 3.6 s or 10 times longer than that from fitting in Figure 9. Trapped electrons do not contribute to the diffusive current and effectively decrease the Spitzer conductivity by a factor  $f(\epsilon) = (1 - 1.80\sqrt{\epsilon} + 0.80\epsilon)$ ; this is about 0.41 times and is included. Because of the large

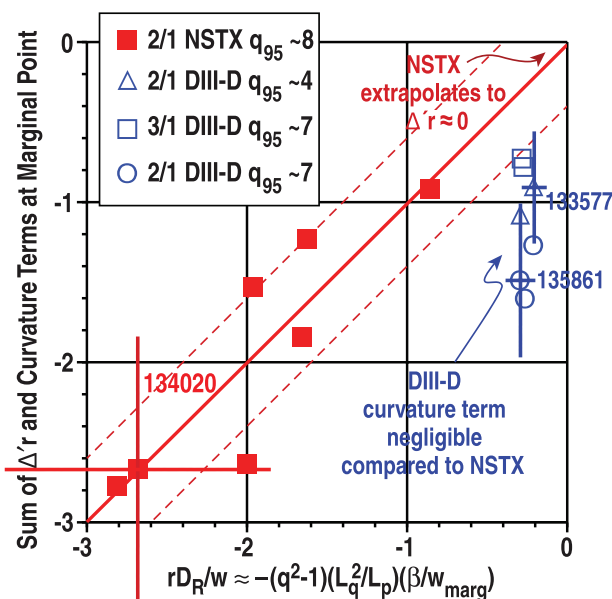


FIG. 8. Same as Fig. 7 but inferred sum of the stabilizing terms plotted versus the independently calculated curvature parameter. The linear fit for NSTX and the  $\pm 1\sigma$  certainties are overlaid.

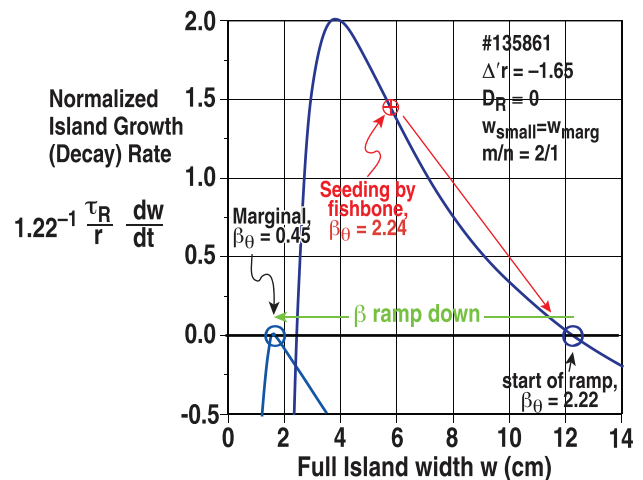


FIG. 9. Evaluation of the MRE for DIII-D  $m/n = 2/1$  case of #135861 from Fig. 3. Fitting at the marginal point with the  $D_R$  term neglected. The same fitting parameters are used for the saturated mode at the start of the NBI ramp at higher beta (except  $w_{small} \propto \beta_{\theta}^{1/2}$  assumed). And in red, the initially growing island width seeded by a fishbone (at similar beta to the start of the ramp) is noted.

hysteresis in DIII-D, if at high beta when the NTM is scaled,  $\Delta r$  is less negative (less stability), the inferred  $\tau_R$  would be longer.

Turning to NSTX, note that with both the  $\Delta'$  term and  $w_{small}$  effects neglected, MRE solutions of the form of Eq. (2.1) with  $\dot{w} = 0$  do not exist. The balance would then have  $0 = C_{Rr}D_R/w + \varepsilon^{1/2}r(L_q/L_{pe})\beta_{\theta e}/w$  which with  $D_R \propto \beta$  and  $\beta \propto \beta_{\theta e}$  has no solution for  $w$ . Even with the  $w_{small}$  effect retained, it is possible to show that there are no solutions of equation (2.1) with  $\Delta' \equiv 0$  that allow  $\dot{w} = 0$  at  $w_{marg}$  and  $\dot{w} < 0$  at all other  $w$ , the form of the MRE we seek to match to experiment. Furthermore, retaining the curvature term  $\propto w^{-1}$  (but still neglecting any dependence of  $\Delta$  on  $w$ ) shifts, the value of  $w_{marg}$  from exactly equal to  $w_{small}$  to a larger value,

$$\frac{w_{marg}^2}{w_{small}^2} = \frac{\varepsilon^{1/2}r(L_q/L_{pe})\beta_{\theta e}}{C_{Rr}D_R + \varepsilon^{1/2}r(L_q/L_{pe})\beta_{\theta e}} > 1, \quad (5.1)$$

noting  $C_{Rr}D_R$  is negative and  $\varepsilon^{1/2}(rL_q/L_{pe})\beta_{\theta e}$  is positive and again assuming  $\Delta' r \neq \Delta' r(w)$ . Operationally, in NSTX, it was actually difficult to routinely strike an  $m/n = 2/1$  mode every shot with the available beam power; thus only these seven discharges are available for analysis in which the mode is excited, and stays in H-mode without wall-locking as beam power is stepped down, and stabilizes. The behavior is thus consistent with the requirement for a positive  $\Delta'$  to establish a metastable space ( $\dot{w} > 0$  for some range in  $w$ ) to be seeded; which then falls back to  $\Delta' < 0$  with the mode stabilizing as beta is reduced. In contrast, in virtually every DIII-D discharge, it was easy to produce the  $m/n = 2/1$  mode but at much higher beta than for self-stabilization.

Fitting an MRE to the NSTX marginal point and to the slightly larger saturated island at the NBI stepdown (at slightly higher  $\beta_{\theta}$ ) constrains the curvature term, the  $\Delta' r$  term

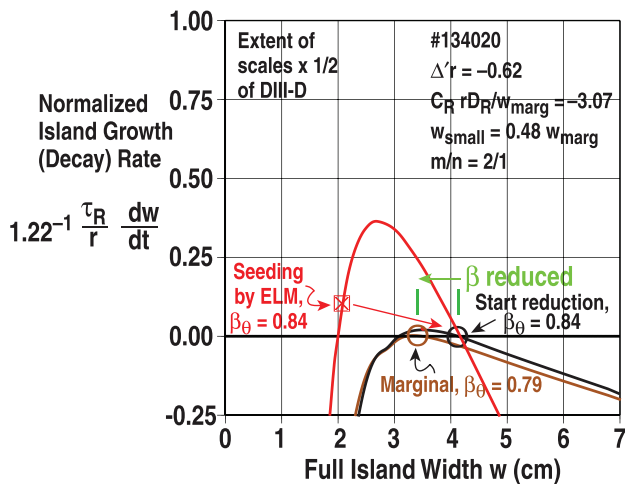


FIG. 10. Evaluation of the MRE for NSTX  $m/n = 2/1$  case #134020 from Fig. 4. Fitting at the marginal point is dominated in stabilization by the curvature term ( $C_{Rr}D_R/w = -3.07$ ) but with a negative  $\Delta'$  ( $\Delta' r = -0.62$ ) retained. The  $w_{small}$  parameter is reduced to  $0.48 w_{marg}$ . The curves (black/brown) for “ $\beta$  reduced” have fixed  $\Delta' r = -0.62$ , and the curve (red) for “seeding by ELM” has  $\Delta' r = 0.62 - 0.30w$ . The label “ $\beta$  reduced” (green) shows the period from the start of the reduction in NBI power to the marginal point.

and the relation of  $w_{marg}$  to  $w_{small}$ . The MRE fit for NSTX is shown in Fig. 10 for the  $m/n = 2/1$  case # 134020. The curvature term is about 5 times as stabilizing as the  $\Delta' r$  term and the small island effect parameterization  $w_{small}$  is about half of the marginal island width [which increases the effective bootstrap term at the marginal point by  $(2/3)/(11/12) \approx 11/8$ ]. Note how close the start of NBI reduction and the marginal point curves are in Fig. 10, which denotes the little hysteresis between saturation and stabilization. NSTX discharge #134020 has the  $m/n = 2/1$  mode seeded by an edge localized mode (ELM) at  $\beta_{\theta} = 0.84$  and an initially growing island of about 2.1 cm at a rate of about 42 cm/s and minor radius  $r \approx 36$  cm. To modify the MRE to allow growth to saturation (at  $w_{sat} \approx 4.2$  cm), an initially positive  $\Delta'$  ( $\Delta' r > 0$ ) must be invoked which goes through zero and then becomes negative as the island grows. The physics in a  $\Delta' r$  of form  $C_0 - C_1 w$  arises from matching outer solutions across the island width rather than for  $w \equiv 0$ , the much narrower tearing layer.<sup>38</sup> Such an NTM mechanism has been observed in Tokamak à Configuration Variable (TCV).<sup>31</sup> This is the red seeding MRE curve in Fig. 10. The value of  $\dot{w}/r$  at  $w_{seed}$  in Figure 10 yields a  $\tau_R$  of about 84 ms. This is about two fifths of the value from resistive diffusion within the rational surface of  $\tau_R \approx 210$  ms, previously discussed. Again, as in DIII-D, the fitted  $\tau_R$  from initial mode growth after seeding is less (or in DIII-D, well less) than that computed from Spitzer resistivity, which includes a trapping correction and a reasonable estimate of  $Z_{eff}$ .

## VI. NIMROD CODE MODULE DIAGNOSTIC CALCULATIONS

The relative importance of the stabilizing curvature in full shaped geometry can be confirmed by diagnostic modules in the NIMROD resistive MHD stability code.<sup>45</sup> MHD equilibrium reconstructions with MSE for the cases of Table I are used as inputs: these include kinetic fits of  $n_e$  and  $T_e$  profiles from Thomson scattering and of  $T_i$  profiles from CER or CHERS. Flux surface averaging is done on the original equilibrium in a separate part of the code, the module “fluxgrid,” and is not looking at the time advance of the fields; this allows calculation of the geometry without doing a time dependent initial value simulation.<sup>46</sup> NIMROD calculates the effective  $m/n = 2/1$  mode bootstrap drive coefficient  $D_{nc}$  in full shaped geometry using the simplified “ $1 \times 1$ ” approximation of Ref. 10; this calculates the bootstrap drive from the electron pressure only and is very close to what was here done analytically as described in Sec. II. NIMROD also calculates the resistive interchange stability parameter  $D_R$  in the full shaped geometry. The stability coefficients that NIMROD is calculating here are also defined in terms of an MRE. This is also laid out in terms that are equivalent to those of the MRE of Eq. (2.1) (which is itself based on analysis on the outboard midplane). The dimensionless form of the MRE in NIMROD is taken as<sup>9,46</sup>

$$\frac{k_0}{\eta^*} \frac{dw}{dt} = \left( \Delta^* + \frac{D_R}{w} \right) + \left( \frac{D_{nc}}{w} + \frac{D_{pol}}{w^3} \right), \quad (6.1)$$

where  $w$  is the full island width in normalized flux space,  $\eta^*$  is the resistive diffusion coefficient in flux space,  $k_0$  is a

TABLE II. NIMROD calculation of terms in the MRE for the cases of Table I for  $m/n = 2/1$ .

|                     | NSTX #134020               | DIII-D #133577               | DIII-D #135861               |
|---------------------|----------------------------|------------------------------|------------------------------|
| $\varepsilon^{1/2}$ | 0.567                      | 0.478                        | 0.402                        |
| $D_R$               | -0.23 (-0.26) <sup>a</sup> | -0.044 (-0.015) <sup>a</sup> | -0.088 (-0.018) <sup>a</sup> |
| $D_R/D_{nc}$        | -0.28                      | -0.18                        | -0.092                       |
| $D_R/(\Delta^* w)$  | 0.72 <sup>b</sup>          | 0.37 <sup>b</sup>            | 0.16 <sup>b</sup>            |

<sup>a</sup>From analytic formula  $D_R \approx (q^2 - 1)(L_q^2/rL_p)\beta$ .

<sup>b</sup>For  $D_{pol}/w^3 = -D_{nc}/3w$  at the marginal point.

constant, and  $D_{pol}$  allows an explicit small island stabilization to be included. Again, note that in this paper, NIMROD is not doing an initial value simulation, but only calculating the terms  $D_R$  and  $D_{nc}$ . NIMROD does not (yet) have a model for evaluating  $D_{pol}$ . Further, NIMROD is not a code that can calculate  $\Delta^*$ ; this must be ported in from a code such as PEST3, beyond the scope of this paper, as already discussed. We have gathered the stabilizing terms in the first set of parentheses, and the destabilizing bootstrap term opposed by small island effects in the second set.

The NIMROD calculations are given in Table II. (These are based on the same cases as in Table I.) The curvature parameter  $D_R$  from NIMROD is actually close to the large aspect ratio expansion analytic formula for NSTX, but NIMROD finds that the  $D_R$  in DIII-D is 3 ~ 5 times a bigger effect than that of the expansion formula, depending on the local  $q$ -surface aspect ratio, which in turn is found to change with  $q_{95}$  (see row 2 of Table II). The large aspect ratio expansion is based on outboard midplane evaluation only and does not take into account the strong shaping (in both elongation and triangularity) that NIMROD does include rigorously.

Curvature stabilization is found by NIMROD to be relatively small in NSTX and to be relatively even smaller in DIII-D as the ratio of  $D_R/D_{nc} \ll 1$ . The computed ratio of  $D_R/D_{nc}$  decreases as  $\varepsilon$  is reduced with  $D_R/D_{nc} \approx -1.8\varepsilon^{1.6}$  (see row 3 of Table II). The large aspect ratio expansion (assuming  $T_i \approx T_e$ ,  $L_{pe} \approx L_p$ ,  $L_q/r \approx 1/2$ , and  $\kappa \approx 1.7$ ) yields an equivalent  $D_R/D_{nc} \approx -1.3\varepsilon^{3/2}$ , which is close to the NIMROD evaluation. Note that when  $D_R/D_{nc} < 1$  (or  $\ll 1$ ), the curvature cannot by itself (absent other effects) obviate the destabilizing bootstrap drive; this is discussed next.

At the marginal point, we can assume as before in Eq. (2.1) that the effective  $D_{pol}/w^3 = -D_{nc}/3w$ . Then to gauge the relative stabilizing effect of the curvature to that of  $\Delta'$ , Eq. (6.1) yields at  $\dot{w} = 0$ ,

$$D_R/\Delta^* w = -1/(1 + 2D_{nc}/3D_R) \quad (6.2)$$

noting  $D_{nc}$  is positive and  $D_R$  and  $\Delta^*$  are assumed negative. This is also given in Table II (see row 4). For these three  $m/n = 2/1$  cases of different  $\varepsilon$ , NIMROD finds that the ratio decreases with reduced  $\varepsilon$  as  $8.9 \varepsilon^{2.2}$ . The NSTX case #134020 evaluated here is found by NIMROD to have a significant but not dominant stabilizing curvature effect comparable to that of a negative  $\Delta'$  (not directly calculated) as previously discussed. In contrast, the MRE analysis used in

Fig. 10 at the marginal point (based on the multi-shot data fit to NSTX in Fig. 8) has the equivalent  $C_R D_R / \Delta' w_{margin} \approx 5$ , i.e., dominated by the curvature term. The DIII-D cases are found by NIMROD to be  $\Delta'$  dominated (3~6 times more stabilizing than the curvature term), justifying the neglecting of  $D_R$  in the fit of Fig. 9.

## VII. DISCUSSION

The excitation, saturation, and self-stabilization (marginal point) of  $m = 2$  or  $3$ ,  $n = 1$  neoclassical tearing modes in DIII-D and NSTX with very different aspect ratio allows examination of two key pieces of physics in NTMs: (1) the scaling of the small island effects that turn off the destabilizing bootstrap drive and (2) the relative importance of the stabilizing effect of good average magnetic field curvature.

Empirically, the marginal island width is found to be 2~3 times the ion banana width, with the ratio increasing with the square root of the local  $q = m/n$  inverse aspect ratio. Comparison to the transport threshold is problematic due to uncertainty over which  $\chi_{\perp}$  to use; the typical equilibrium gyroBohm transport does not have a radial step size smaller than the marginal island, thus is not diffusive. Further,  $w_d$  using gyroBohm is both too small compared to (and does not scale as)  $\varepsilon^{1/2} \rho_{0i}$ . The polarization threshold as an explanation of the small island physics is also questionable. Theory requires island propagation in the plasma frame to be between zero and the ion diamagnetic drift frequency for helical polarization current to be stabilizing. However, within experimental uncertainties, propagation is found to be zero or slightly in the electron diamagnetic drift frequency direction. This may be due to the relatively high ion collisionality  $\nu_i/\varepsilon$  with respect to the magnitude of the electron drift frequency  $\omega_e^*$  at the marginal point ranging from  $\lesssim 1 \lesssim 3$ , a subject for future exposition. However, including the effect of high collisionality enhancement of the ion polarization current and ignoring the flow yields a fair agreement of the experimental ratio of the marginal island width to the ion banana width with polarization theory.

The evaluation of the destabilizing helically perturbed bootstrap current with small island effects yields the sum of the stabilizing classical tearing ( $\Delta'$ ) and curvature ( $D_R$ ) effects. Lacking a tractable means to measure  $\Delta'$  directly or reliably calculate it from an MHD equilibrium reconstruction, the sum is separated first by comparing the scaling with a curvature parameter. The good linear correlation for NSTX extrapolates to  $\Delta' \approx 0$ , which allows separation. Further empirical analysis indicates that for DIII-D, the curvature effect is much smaller and that negative  $\Delta'$  dominates the sum of the two terms. This separation also readily explains the very different behavior of the  $n = 1$  NTMs from onset to saturation to stabilization with beta in that there is little hysteresis in NSTX and there is large hysteresis in DIII-D. Second, the size of and the relative importance of the curvature effect in relation to the bootstrap drive is computed in full geometry by the resistive MHD stability code NIMROD. The strong  $\varepsilon^{3/2}$  scaling predicted by the large aspect ratio approximation of  $D_R$  is confirmed by NIMROD. The MRE balance at the marginal point in a NIMROD formalism shows that the

curvature stabilization is relatively unimportant in the large aspect ratio DIII-D; for NSTX, NIMROD analysis of a typical discharge suggests curvature is almost as important as a negative  $\Delta'$  at the marginal point, however not dominant as in the multi-discharge empirical analysis.

Advantages at low aspect ratio are confirmed of both a relatively larger characteristic small island for stabilization and the presence of a significant stabilizing curvature effect. Both together should tend to make NTMs harder to excite. A stabilizing curvature effect could maintain NTM stability of an equilibrium which is even classically unstable, i.e.,  $\Delta' > 0$ .

## ACKNOWLEDGMENTS

Thanks to Scott Kruger of the Tech-X Corp. for discussions on the NIMROD code. This work was supported in part by the U.S. Department of Energy under DE-FG02-04ER54698, DE-AC02-09CH11466, and DE-FG02-04ER54761. Thanks to the DIII-D and NSTX Teams.

- <sup>1</sup>J. Wesson, *Tokamaks*, 2nd ed. (Clarendon, Oxford, 1997), pp. 124–131 and 166–168.
- <sup>2</sup>O. Sauter, C. Angioni, and Y. R. Lin-Liu, *Phys. Plasmas* **6**, 2834 (1999) [erratum *Phys. Plasmas* **9**, 5140 (2002)].
- <sup>3</sup>W. X. Qu and J. D. Callen, “Nonlinear growth of a single neoclassical MHD tearing mode in a tokamak,” University of Wisconsin Report UWPR 85-5, 1985.
- <sup>4</sup>R. Carrera, R. D. Hazeltine, and M. Kotschenreuther, *Phys. Fluids* **29**, 899 (1986).
- <sup>5</sup>J. D. Callen, W. X. Qu, K. D. Siebert, B. A. Carreras, K. C. Shaing, and D. A. Spong, *Plasma Physics and Controlled Nuclear Fusion Research* (IAEA, Vienna, 1987), Vol. 2, p. 157.
- <sup>6</sup>R. J. La Haye, *Phys. Plasmas* **13**, 055501 (2006).
- <sup>7</sup>A. H. Glasser, J. M. Greene, and J. L. Johnson, *Phys. Fluids* **18**, 875 (1975).
- <sup>8</sup>A. H. Glasser, J. M. Greene, and J. L. Johnson, *Phys. Fluids* **19**, 567 (1976).
- <sup>9</sup>S. E. Kruger, C. C. Hegna, and J. D. Callen, *Phys. Plasmas* **5**, 455 (1998).
- <sup>10</sup>C. C. Hegna, *Phys. Plasmas* **6**, 3980 (1999).
- <sup>11</sup>H. Lütjens, J. F. Luciani, and X. Garbet, *Phys. Plasmas* **8**, 4267 (2001).
- <sup>12</sup>R. Fitzpatrick, *Phys. Plasmas* **2**, 825 (1995).
- <sup>13</sup>N. N. Gorelenkov, R. V. Budny, Z. Chang, M. V. Gorelenkova, and L. E. Zakharov, *Phys. Plasmas* **3**, 3379 (1996).
- <sup>14</sup>A. B. Mikhailovskii, M. S. Shirokov, V. S. Tsypin, S. V. Konovalov, T. Ozeki, T. Takizuka, R. M. O. Galvao, and I. C. Nascimento, *Phys. Plasmas* **10**, 3975 (2003).
- <sup>15</sup>M. Sato and M. Wakatani, *Nucl. Fusion* **45**, 143 (2005).
- <sup>16</sup>H. R. Wilson, M. Alexander, J. W. Connor, A. M. Edwards, D. Gates, O. Gruber, R. J. Hastie, C. C. Hegna, T. C. Hender *et al.*, *Plasma Phys. Controlled Fusion* **38**, A149 (1996).
- <sup>17</sup>F. L. Waelbroeck, J. W. Connor, and H. R. Wilson, *Phys. Rev. Lett.* **87**, 215003 (2001).
- <sup>18</sup>R. J. La Haye, C. C. Petty, E. J. Strait, F. L. Waelbroeck, and H. R. Wilson, *Phys. Plasmas* **10**, 3644 (2003).
- <sup>19</sup>E. Poli, A. G. Peeters, A. Bergmann, S. Günter, and S. D. Pinches, *Phys. Rev. Lett.* **88**, 075001 (2002).
- <sup>20</sup>R. J. Buttery, O. Sauter, R. Akers, M. Gryaznevich, and R. Martin *et al.*, *Phys. Rev. Lett.* **88**, 125005 (2002).
- <sup>21</sup>R. J. Buttery, R. Akers, E. Arends, N. J. Conway, G. F. Counsell, G. Cunningham, C. G. Gimblett, M. Gryaznevich, and R. J. Hastie *et al.*, *Nucl. Fusion* **44**, 1027 (2004).
- <sup>22</sup>O. Sauter *et al.*, *Phys. Plasmas* **4**, 1654 (1997).
- <sup>23</sup>H. Zohm, D. A. Gates, H. R. Wilson, G. Gantenbein, O. Gruber, S. Günter, M. Maraschek, A. W. Morris, M. Sokoli, D. Wagner, ASDEX Upgrade Team, and COMPASS-D Team, *Plasma Phys. Controlled Fusion* **39**, B237 (1997).
- <sup>24</sup>D. A. Gates, B. Lloyd, A. W. Morris, G. McArdle, M. O’Brien, M. Valovic, C. D. Warrick, H. R. Wilson, and COMPASS-D and ECRH Teams, *Nucl. Fusion* **37**, 1593 (1997).
- <sup>25</sup>R. J. La Haye and O. Sauter, *Nucl. Fusion* **38**, 987 (1998).
- <sup>26</sup>A. Isayama, Y. Kamada, T. Ozeki, and N. Ise, *Plasma Phys. Controlled Fusion* **41**, 35 (1999).
- <sup>27</sup>JET Team (prepared by G. T. A. Huysmans), *Nucl. Fusion* **39**, 1965 (1999).
- <sup>28</sup>H. R. Koslowski, G. Fuchs, R. Jaspers, A. Kramer-Flecken, A. M. Messiaen, J. Ongena, J. Rapp, F. C. Schuller, and M. Z. Tokar, *Nucl. Fusion* **40**, 821 (2000).
- <sup>29</sup>R. J. La Haye, R. J. Buttery, S. Günter, G. T. A. Huysmans, M. Maraschek, and H. R. Wilson, *Phys. Plasmas* **7**, 349 (2000).
- <sup>30</sup>D. A. Kislov, Yu. V. Esipchuk, N. A. Kirnova, I. V. Kliamanov, Yu. D. Pavlov, A. A. Subbotin, V. V. Alikae, A. A. Borshegovskiy, Yu. V. Gott, A. M. Kakurin, S. V. Krilov, T. B. Myalton, I. N. Roy, E. V. Trukhina, V. V. Volkov, and T-10 Team, *Nucl. Fusion* **41**, 1619 (2001).
- <sup>31</sup>H. Reimerdes, O. Sauter, T. Goodman, and A. Pochelon, *Phys. Rev. Lett.* **88**, 105005 (2002).
- <sup>32</sup>R. J. La Haye, R. Prater, R. J. Buttery, N. Hayashi, A. Isayama, M. E. Maraschek, L. Urso, and H. Zohm, *Nucl. Fusion* **46**, 451 (2006).
- <sup>33</sup>L. Urso, H. Zohm, A. Isayama, M. Maraschek, E. Poli, ASDEX Upgrade Team, and JT-60 Team, *Nucl. Fusion* **50**, 025010 (2010).
- <sup>34</sup>P. Maget, H. Lütjens, R. Coelho, B. Alper, M. Brix, P. Buratti, R. J. Buttery, E. De la Luna, N. Hawkes *et al.*, *Nucl. Fusion* **50**, 045004 (2010).
- <sup>35</sup>R. J. La Haye, D. P. Brennan, R. J. Buttery, and S. P. Gerhardt, *Phys. Plasmas* **17**, 056110 (2010).
- <sup>36</sup>R. J. La Haye, C. C. Petty, P. A. Politzer, and DIII-D Team, *Nucl. Fusion* **51**, 053013 (2011).
- <sup>37</sup>C. M. Bishop, J. W. Connor, R. J. Hastie, and S. C. Cowley, *Plasma Phys. Controlled Nucl. Fusion* **33**, 389 (1991).
- <sup>38</sup>C. C. Hegna and J. D. Callen, *Phys. Plasmas* **1**, 2308 (1994).
- <sup>39</sup>C. C. Petty, T. C. Luce, R. I. Pinsker, K. H. Burrell, S. C. Chiu *et al.*, *Phys. Rev. Lett.* **74**, 1763 (1995).
- <sup>40</sup>A. Kuritsyn, M. Yamada, S. Gerhardt, H. Ji, R. Kulsrud, and Y. Ren, *Phys. Plasmas* **13**, 055703 (2006).
- <sup>41</sup>C. C. Petty, M. E. Austin, C. T. Holcomb, R. J. Jayakumar, R. J. La Haye *et al.*, *Phys. Rev. Lett.* **102**, 045005 (2009).
- <sup>42</sup>F. L. Hinton and R. D. Hazeltine, *Rev. Mod. Phys.* **48**, 239 (1976).
- <sup>43</sup>Z. Chang, J. D. Callen, E. D. Fredrickson, R. V. Budny, C. C. Hegna *et al.*, *Phys. Rev. Lett.* **74**, 4663 (1995).
- <sup>44</sup>M. S. Chu, R. J. La Haye *et al.*, *Phys. Plasmas* **9**, 4584 (2002).
- <sup>45</sup>C. R. Sovinec, T. A. Gianakon, E. D. Held, S. E. Kruger, D. D. Schnack, and NIMROD Team, *Phys. Plasmas* **10**, 1727 (2003).
- <sup>46</sup>D. P. Brennan, E. J. Strait, A. D. Turnbull, M. S. Chu, R. J. La Haye *et al.*, *Phys. Plasmas* **9**, 2998 (2002).